Electronic Supplementary Information for

Electron Interaction between Ligand and PdAg Nanowire Networks Tunes Formic Acid Dehydrogenation Catalysis

Hu Liu,[a#] Bolong Huang,[b#] Kai Wang,[c] Yongsheng Yu,[a*] Weiwei Yang,[a*] and Shaojun Guo [c*]

[a] MIIT Key Laboratory of Critical Materials Technology for New Energy Conversion and Storage, School of Chemistry and Chemical Engineering, Harbin Institute of Technology, Harbin, Heilongjiang 150001, China

[b] Department of Applied Biology and Chemical Technology, The Hong Kong Polytechnic University, Hung Hom, Kowloon, Hong Kong SAR, China

[c] Department of Materials Science & Engineering, College of Engineering, Peking University, Beijing 100871, China

[#] These authors contribute equally.

*To whom correspondence should be addressed. Email: ysyu@hit.edu.cn, yangww@hit.edu.cn and guosj@pku.edu.cn

Supplementary Methods

Chemicals and Materials. Silver nitrate ($AgNO_3$), palladium (II) nitrate dihydrate ($Pd(NO_3)_2\cdot 2H_2O$), formic acid (HCOOH) and poly-*n*-vinylpyrrolidone (PVP, M_w = 58000) were purchased from Aldrich Company, USA. The distilled water (18 MΩ/cm) was supplied by a Water Purifier Nanopure water system. Sodium hydroxide (NaOH, A. R. grade, Tianjin Chemical Reagent), sodium sulphide (Na_2S, A. R. grade, Tianjin Chemical Reagent), 1, 3-butylene glycol (1, 3-BG, A. R. grade, Tianjin Chemical Reagent), ethanol (C_2H_5OH, A. R. grade, Tianjin Chemical Reagent) and ethylene glycol (EG, A. R. grade, Tianjin Chemical Reagent) were used as received without further purification.

Synthesis of PVPI. In a typical synthesis, the polyvinylpyrrolidine imine (PVPI) was synthesized by ketoamine condensation reaction between PVP and ammonium hydroxide ($NH_3\cdot H_2O$). Briefly, a 10 mL 1, 3-BG solution including 1.2 mmol PVP (133.2 mg, M_W = 58000, calculated in terms of the repeating unit) in a 50 mL two-neck flask was heated with an oil bath at 170 ^oC for 10 min. Then 0.5 mL ammonium hydroxide (25 %) was then quickly injected into the 1, 3-BG solution using a pipette, followed by immediately sealing the exit of two-neck flask and reflux pipe. After refluxing for 2 h, the clear solution turned yellow. Then 1, 3-BG was evaporated by reduced pressure distillation at 180 ^oC, and the yellow production was dried in vacuum drier at 160 ^oC for 2 h to remove residual 1,3-BG. The final yellow production (PVPI) was obtained.

Synthesis of PVPI-capped networked Pd_5Ag_5 NWs. In a typical process, 10 mL of 1, 3-BG and 1.2 mmol of PVP (133.2 mg, M_W = 58,000, calculated in terms of the repeating unit) were added into a 50 mL two-neck flask heated with an oil bath at 170 ^oC for 10 min. Then, 0.5 mL ammonium hydroxide (25 %) was then quickly injected into the 1, 3-BG solution using a pipette, followed by immediately sealing the exit of two-neck flask and reflux pipe. After refluxing for 2 h, the clear solution turned yellow. The above reaction system was refluxed for 0.5 h at 170 ^oC to remove ammonium hydroxide and water. Then, 0.5 mL Na_2S solution (1 mM in EG) was quickly injected into the 1, 3-BG solution using a pipette. After 5 min, $AgNO_3$ (0.1 mmol, 16.99 mg) and $Pd(NO_3)_2\cdot 2H_2O$ (0.1 mmol, 26.64 mg) co-dissolved in 4 mL of distilled water at room temperature were quickly injected into the stirring 1, 3-BG solution using a syringe. After the reaction for 2 h, the solution was cooled down to room temperature. The as-synthesized PVPI-capped networked Pd_5Ag_5 NWs were purified at least three times with 60 mL acetone and 3 mL water. The final black precipitation was redispersed into 9.6 mL distilled water for further catalyst evaluation. The PVPI-capped networked PdAg NWs (Ag, Pd, Pd_7Ag_3 and Pd_3Ag_7) with other compositions were also synthesized by same method by controlling metal precursors at the Pd/Ag ratios of 0:10, 10:0, 7:3 and 3:7, respectively. In addition, PVP-capped networked Pd_5Ag_5 NWs were prepared also by co-reduction process of $AgNO_3$ and $Pd(NO_3)_2\cdot 2H_2O$ precursor in the above solution system without ammonium hydroxide.

Characterizations. X-ray diffraction (XRD) was carried out on a Bruker AXS D8-Advanced diffractometer with Cu K_α radiation (λ =1.5418 Å). The composition analyses of the samples were carried on FEI Nova Nano SEM450 with energy dispersive spectroscopy (EDS) and an inductively coupled plasma optical emission spectrometer (ICP-AES) (Perkin Elmer, Model Optima 5300DV, USA). Samples for TEM analysis were prepared by depositing a single drop of diluted networked Pd_5Ag_5 NWs catalyst dispersion in ethanol on amorphous carbon coated copper grids. TEM images were obtained with a Philips CM 20 operating at 120 kV. High-resolution TEM (HRTEM) and high-angle annular dark field (HAADF) images were obtained on a Fei Tecnai Osiris with an accelerating voltage of 200 kV. X-ray photoelectron spectroscopy (XPS) measurement was performed on an ESCALAB-MKII spectrometer (Thermo Fisher Scientific) with Al K_α X-ray radiation as the X-ray source for excitation. The UV/Vis spectra were recorded on a Perkin Elmer Lambda 35 spectrometer. The infrared spectra were recorded on a Bruker Tensor 27 FTIR spectrometer. ^1H NMR spectra were performed on an INOVA-400 NMR spectrometer with $CDCl_3$-d6 as solvent. Detailed analyses for

CO_2, H_2 and CO were performed on GC-6890 with thermal conductivity detector (TCD) and flame ionization detector (FID)-Methanator (detection limit for CO: ~ 2 ppm).

The PVPI-capped networked Pd_5Ag_5 NWs Catalyst Evaluation. The catalytic activities of the different composition PVPI-capped networked PdAg NWs (Ag, Pd, Pd_7Ag_3, Pd_5Ag_5, and Pd_3Ag_7) for FA dehydrogenation in water were determined by measuring the rate of gas (CO_2 + H_2) evolved in a typical gas burette system. Before the test, the PVPI-capped networked Pd_5Ag_5 NWs catalyst (0.1 mmmol) was dispersed in 9.6 mL of water *via* sonication and transferred into a two-neck round bottom flask (25 mL) containing a teflon-coated stir bar. One neck was connected to a gas burette, and the other neck was sealed rubber stopper to introduce FA (0.4 mL). Next, the aqueous dispersion of PVPI-capped networked Pd_5Ag_5 NWs catalyst was stirred with magnetic stirring (600 r/min) at least 15 min in the reaction flask for keeping a constant temperature. Finally, when the desired amount of FA was rapidly injected into the flask using a syringe from the rubber stopper neck under a stirring rate of 600 rpm. The gas volume generated was recorded at certain time intervals. For the PVPI-capped networked PdAg NWs photocatalytic evaluation, we put the above reactor into a black box with 50 W (power input) UV lamp emitting at 365 nm.

CO_2 Removal from H_2/CO_2 Mixture. The molar ratio of CO_2 / H_2 was tested through a NaOH trap absorbing the CO_2.[1] In the experiment, the gas burette system was modified by placing a trap (10 M NaOH solution) between the reaction flask and gas burette. The generated gas mixture passed the NaOH trap, and the CO_2 was captured. The volume of gas generated from NaOH trap was compared with the volume of gas generated from without NaOH trap in FA (1 M, 10 mL) hydrogen generation system in water.

Calculation Summary. In the realistic nanomaterials, the local structures of PdAg nanowire systems are very different. The experimentally reported structures are dominantly based on the surface spontaneously containing Pd and Ag. Thus, to straightforwardly illustrate the physicochemical trend, we simply modeled the PdAg system on the (100) surface of *fcc*-PdAg (within *P4/mmm*) models using the cubic lattice replaced with the same space group of either *fcc*-Pd or *fcc*-Ag but with cut-off at the layer boundary.

We used the CASTEP code to perform our DFT+U calculations.[2] In this framework, we use the rotationally invariant (Anisimov type) DFT+U functional[3] and the Hubbard U parameter self-consistently determined for the pseudized Pd-*4d* and Ag-*4d* orbital by our new linear response method,[4] which have been already successfully reflecting the electron-electron Coulomb potential for the *p*-, *d*- and f-orbital electrons of the semi-core orbital based sulfides should be considered when using DFT+U.[3-9] The geometry optimization used the Broyden-Fletcher-Goldfarb-Shannon (BFGS) algorithm through all calculations.

The PBE functional was chosen for PBE+U calculations with a kinetic cutoff energy of 750 eV, with the valence electron states expressed in a plane-wave basis set. The ensemble DFT (EDFT) method of Marzari *et al.*[10] was used for convergence. The supercell of *fcc*-PdAg (100) surface model was chose as 3×3×1 with sizes of 108 atoms (*i.e.* $Pd_{54}Ag_{54}$), and is established with 6-layer thick. The vacuum thickness is set to be 15 Å. We only allow the top two layers to be varied freely. The reciprocal space integration was performed using the mesh of 2×2×1[11] with Gamma-center-off, which was self-consistently selected for total energy minimization. With these special *k*-points, the total energy is converged to less than $5.0x10^{-7}$ eV per atom. The Hellmann-Feynman forces on the atom were converged to less than 0.001 eV/Å.

As to the pseudopotentials, we know that the norm-conserving pseudopotentials can reflect all-electron behavior for outer shell valence electrons for **|S-matrix|**=1, unlike the ultrasoft pseudopotentials.[12,13] Therefore, the non-linear core corrected norm-conserving pseudopotential can provide a better response in DFT+U calculations, especially for the calculations of defects.[5] We note that our method actually provides almost identical values of the U parameter for both norm-conserving and ultrasoft pseudopotentials. This means that the obtained value has an intrinsic physical meaning for the studied materials. Meanwhile, this will help us to reflect all-electron behavior of the valence electrons especially for the subtle effect of the *4d* electrons and outter *5s* electrons.

The Pd and Ag norm-conserving pseudopotentials are generated using the OPIUM code in the Kleinman-Bylander projector form,[14] and the non-linear partial core correction[15] and a scalar relativistic averaging scheme[16] are used to treat the spin-orbital coupling effect. For this treatment, we actually similarly choose non-linear core correction technique for correcting the valence-core charge density overlapping in such heavy fermions elements, the detail discussion of such method has been presented in previous work about the native point defect study of CeO_2.[5,6] In particular, we treated the (4*d,* 5*s*, 5*p*) states as the valence states of both Pd and Ag atoms. The RRKJ method is chosen for the optimization of the pseudopotentials.[17]

Prior to ab-initio predictions of the Hubbard U on orbitals, the geometries and lattice parameters of all PdAg structural models were optimized using PBE functional calculations. This procedure reduces the computational cost and ensures the reliability of the Hubbard U value obtained by our self-consistent iterative calculations. We use this procedure before the Hubbard U determination because DFT has been already verified to be reliable for the structural optimization of compound solids even with *4f* or *5f* orbitals,[18] even with ultrasoft pseudopotentials. This may be due to the well-developed pseudopotential technique[5,6,18] and, more importantly, to the fact that the electrons on semi-core orbitals have a small influence on the lattice parameters when treated as valence electrons, as shown by the small difference of the DFT and DFT+U calculated lattice parameters.[4-6,19,20] Nevertheless, the U parameter must be determined more carefully. [4-6,19,20]

For the all of the electronic states calculations in PdAg models, we use the self-consistent determination for the U correction on the localized *4d* orbitals to correct the on-site Coulomb energy of the electron spurious self-energy. By that method, the Hubbard U parameters on the half-filled shell of $4d^{10}$ orbitals of Pd is self-consistently determined to be U_d=4.04 eV, and U_d=5.58 eV for Ag-$4d^{10}$. The detail process was referred to the previous work. With our self-consistently determination process, the on-site Hubbard U parameters for 4d of Pd and Ag sites are obtained respectively.

With the above preliminary structure determination, the corresponding electronic structure is further estimated with anisimov-type rotational invariant DFT+U method with CASTEP code.[3] We previously devised a method to ab-initially determine the semicore *d*/*f* orbital energy in order to further self-consistently correct the electronic structures from routine first-principles calculations.[4,21] Our work shows that the method is particularly valid for those materials synthesized *via* the extremely physical or chemical conditions.[4,21] The Hubbard U parameter has been self-consistently determined based on our previous developed method.[4,21] Herein, we utilized this method to ultimately reflect the total energy of the specifically targeted orbital especially with electronic occupation under a variety case of chemical bonding. With chosen ab-initio generated norm-conserving pseudopotentials by OPIUM code, we projected out the two Hubbard potential components on the orbitals by linear response method. One is the orbital chemical potential, and another is the pseudo-charge induced perturbed potential. This method has been further developed to determine the onsite Coulomb type screened Hubbard potential of orbitals.[4,21] The Hubbard potentials for the Pd-*4d* and Ag-*4d* orbitals have been determined in following **Figure S19**.

Supplementary Figures and Tables

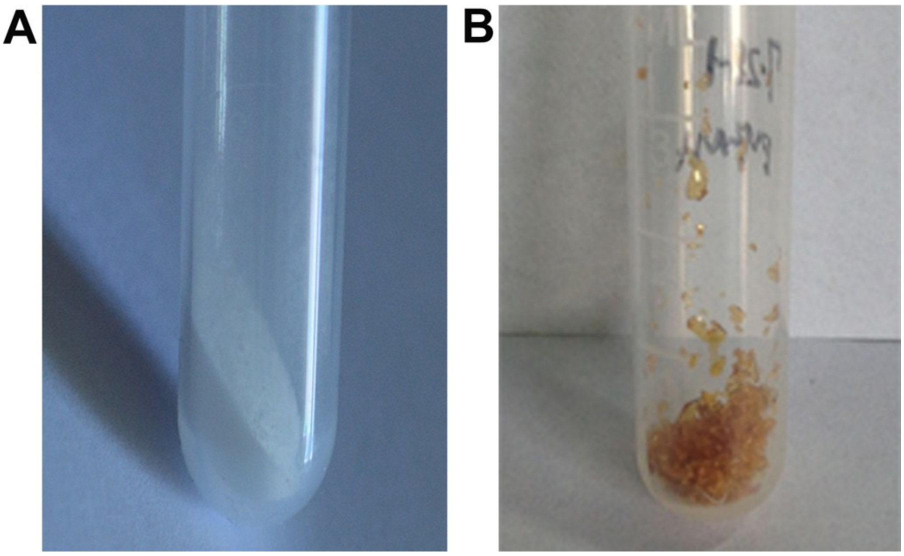

Figure S1. The photographs of (**A**) PVP and (**B**) PVPI.

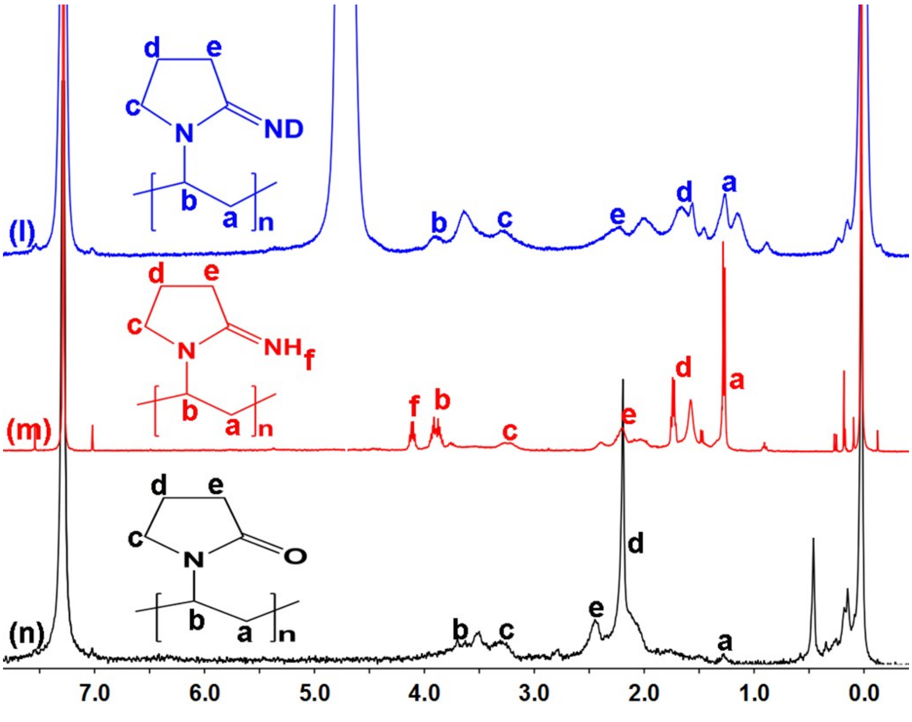

Figure S2. The ^{1}H NMR spectra of the (**l**) PVPI in the D_2O, (**m**) PVPI and (**n**) PVP in the $CDCl_3$.

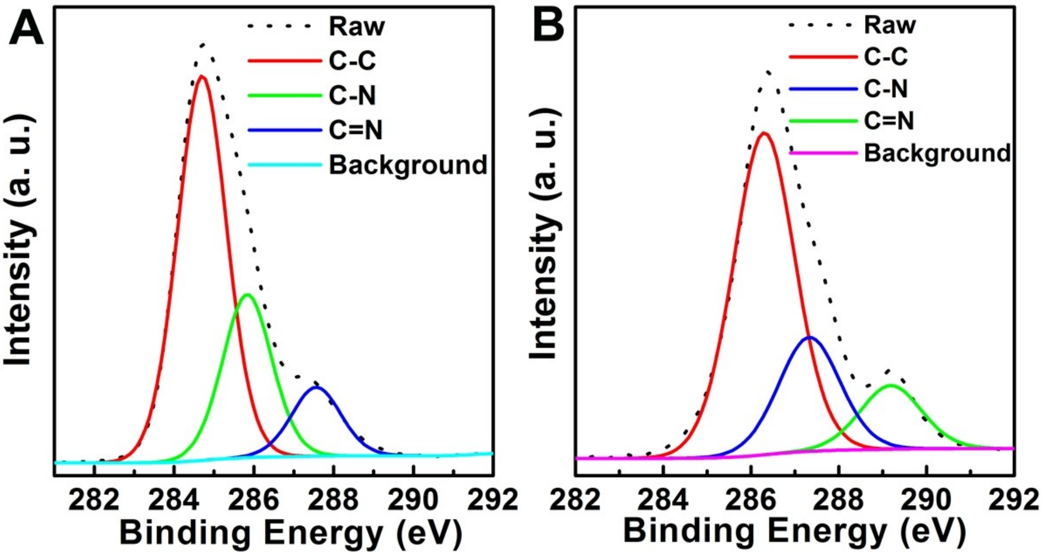

Figure S3. High resolution XPS spectra of C1s for (**A**) PVPI and (**B**) PVPI-capped networked Pd_5Ag_5 NWs.

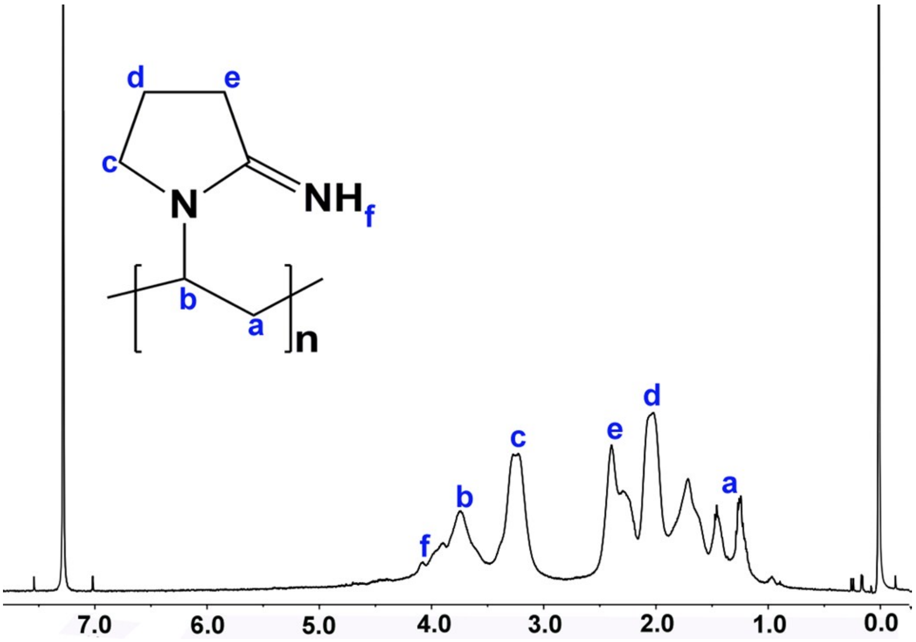

Figure S4. The ^1H NMR spectra of the PVPI-capped networked Pd_5Ag_5 NWs in the $CDCl_3$.

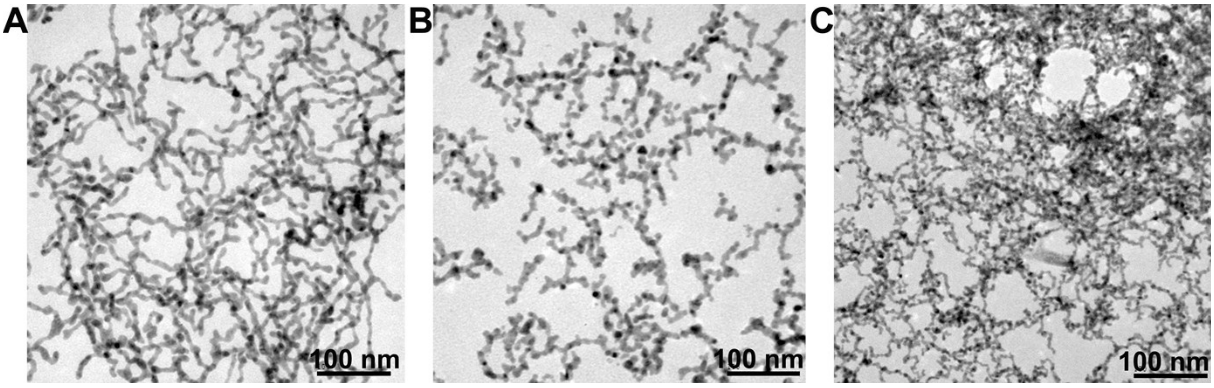

Figure S5. TEM images of **(A)** PVPI-capped networked Pd_3Ag_7, **(B)** Pd_7Ag_3 and **(C)** Pd NWs.

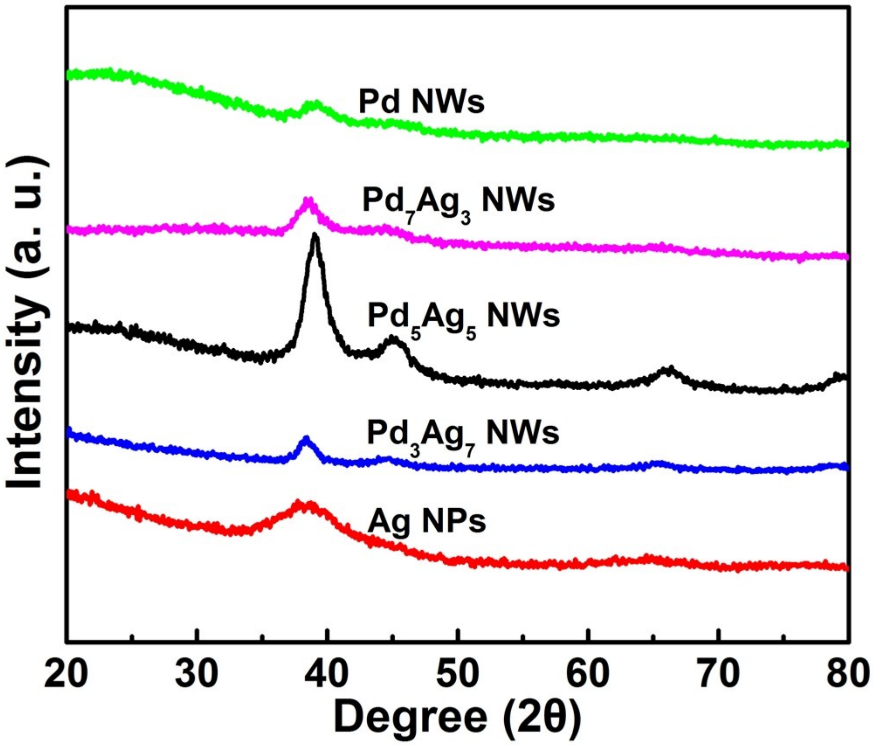

Figure S6. XRD patterns of the Ag NPs, PVPI-capped networked Pd and PdAg NWs.

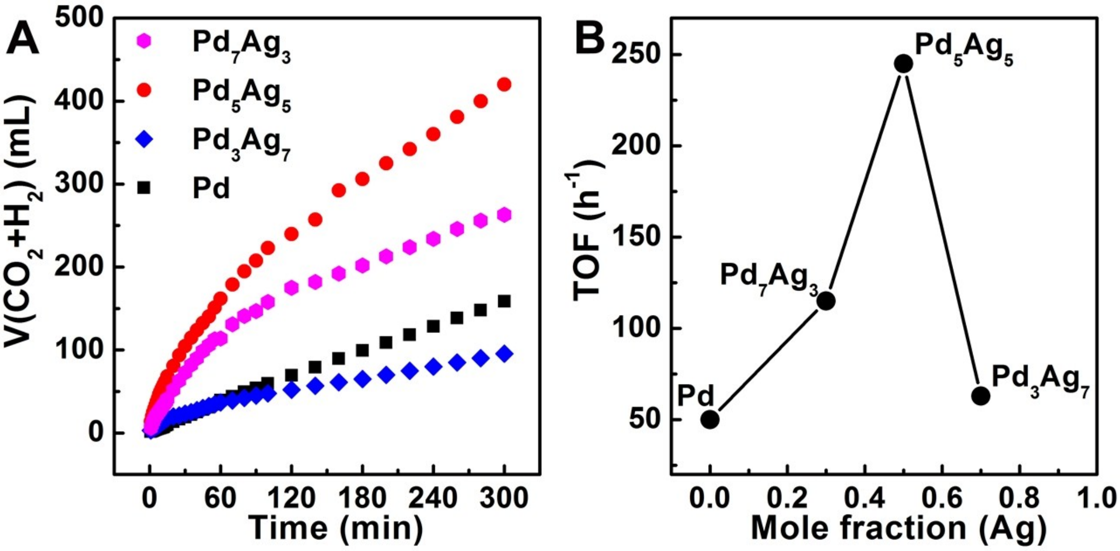

Figure S7. (**A**) The volume of $CO_2 + H_2$ generated *vs.* time from FA hydrogenation system in the presence of different PVPI-capped networked PdAg NWs catalysts in 10 mL FA aqueous solution (1 M) at 25 °C. The initial TOFs of PVPI-capped networked Pd_3Ag_7, Pd_5Ag_5, Pd_7Ag_3 and Pd NWs are 45, 242, 133, and 44 h^{-1}, respectively. (**B**) TOF *vs.* mole fraction of Ag for the PVPI-capped networked PdAg NWs catalysts at different Ag/Pd compositions.

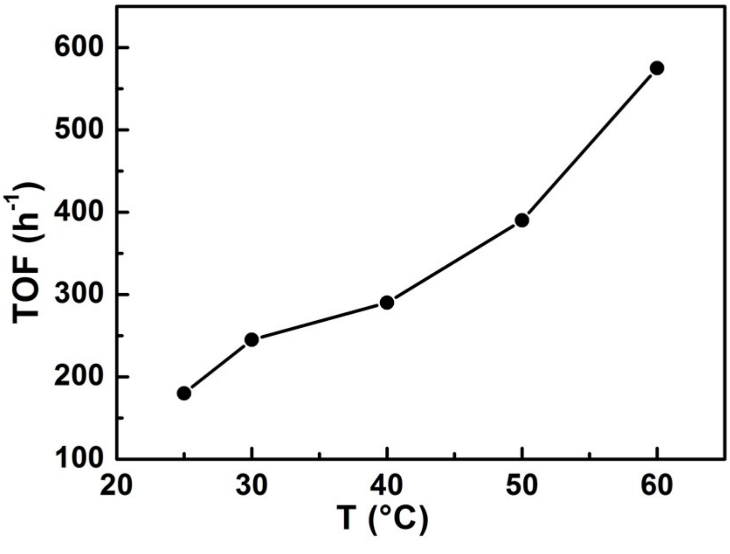

Figure S8. TOF of the FA dehydrogenation catalyzed by PVPI-capped networked PdAg NWs at different temperatures.

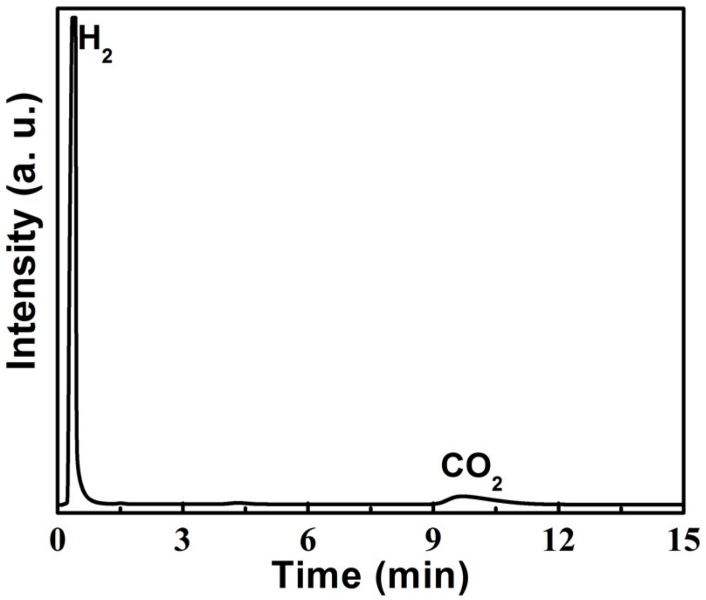

Figure S9. GC spectrum using TCD for the evolved gas from FA (1 M, 10 mL) over PVPI-capped networked Pd_5Ag_5 NWs at 25 °C.

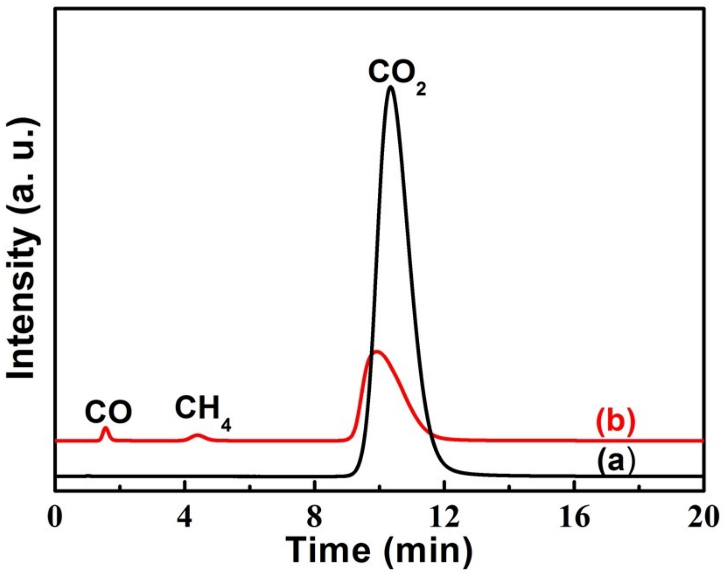

Figure S10. GC spectrum using FID-Methanator for (**a**) the evolved gas from FA (1 M, 10 mL) over PVPI-capped networked Pd_5Ag_5 NWs at 25 °C, and (**b**) reference gas (H_2, 48.88 %; CO, 1.00 %; CH_4, 1.01 %; CO_2, 49.11 %).

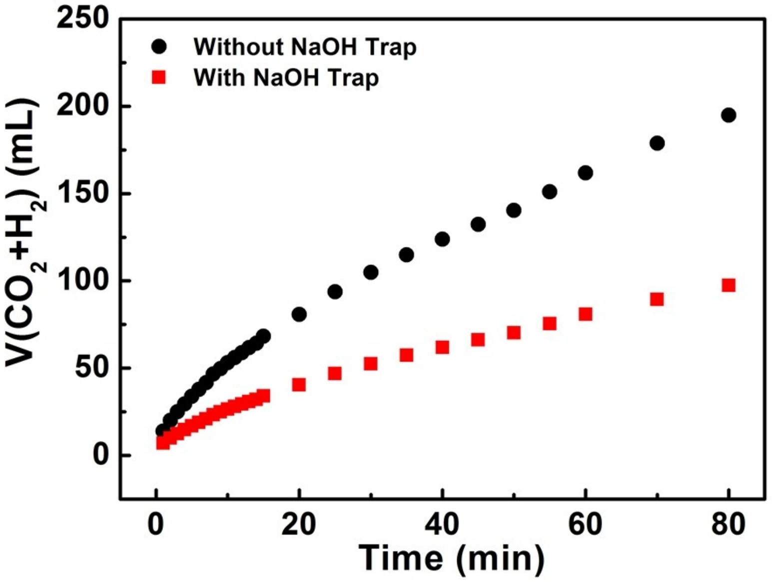

Figure S11. The comparison of the volume of gas generated during PVPI-capped networked Pd_5Ag_5 NWs catalyzed dehydrogenation of aqueous FA solution (10 mL, 1 M) with and without NaOH trap.

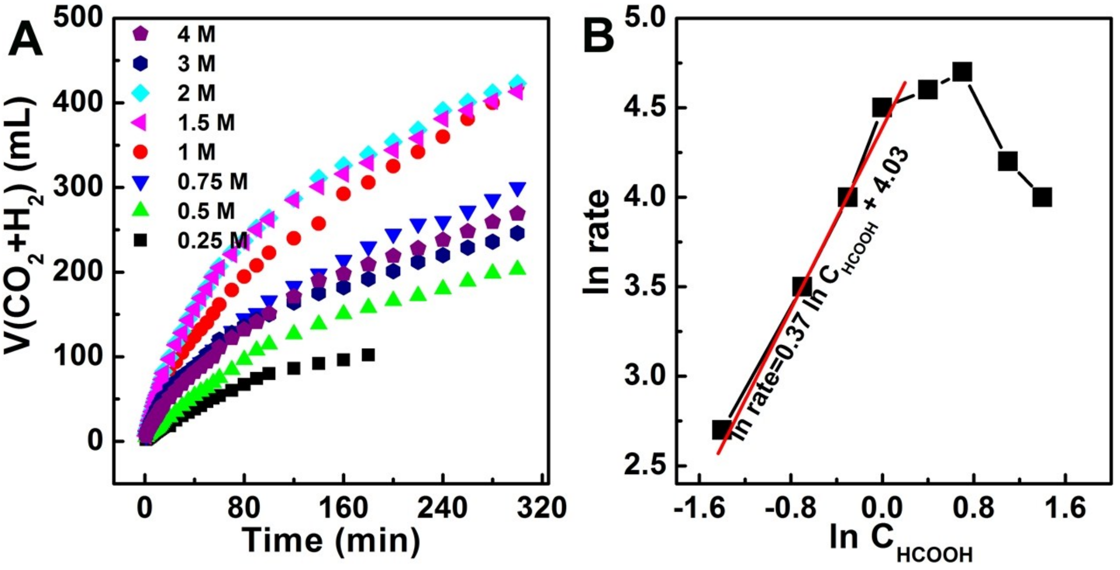

Figure S12. (**A**) CO_2 + H_2 volume generated *vs.* time for the catalytic dehydrogenation of FA at different FA concentrations, and (**B**) the plot of gas generation rate *vs.* FA concentration (both in logarithmic scale).

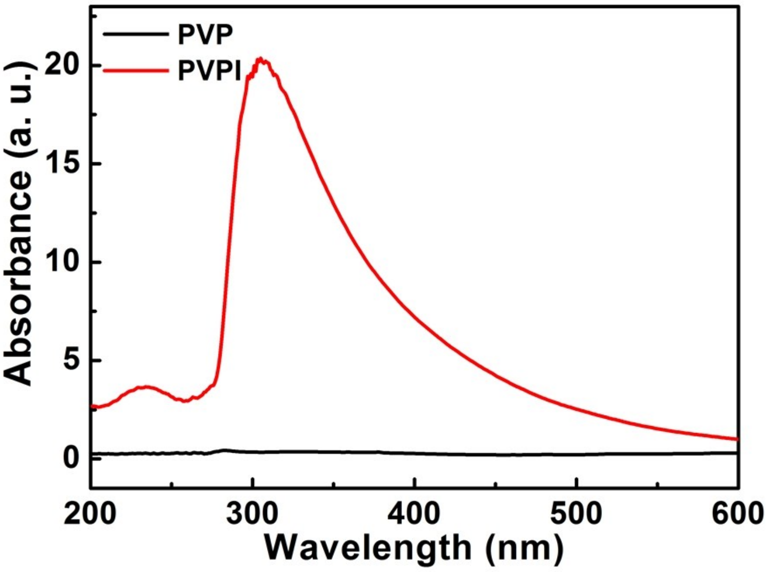

Figure S13. UV-vis spectra of PVP and PVPI in aqueous solution.

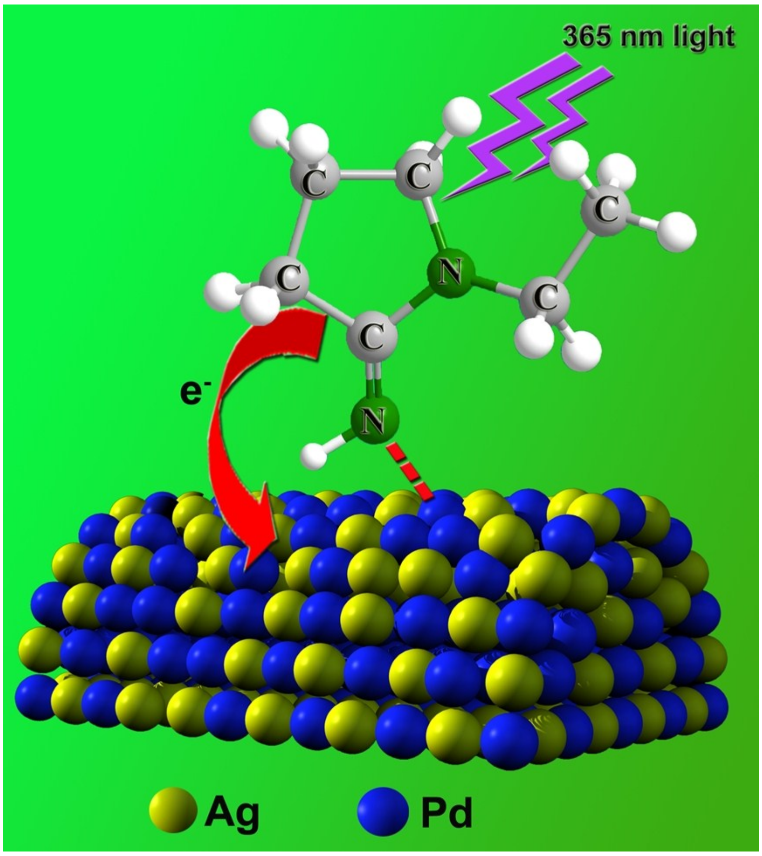

Figure S14. Schematic illustration of electron transfer on the surface of PVPI-capped networked Pd_5Ag_5 NWs.

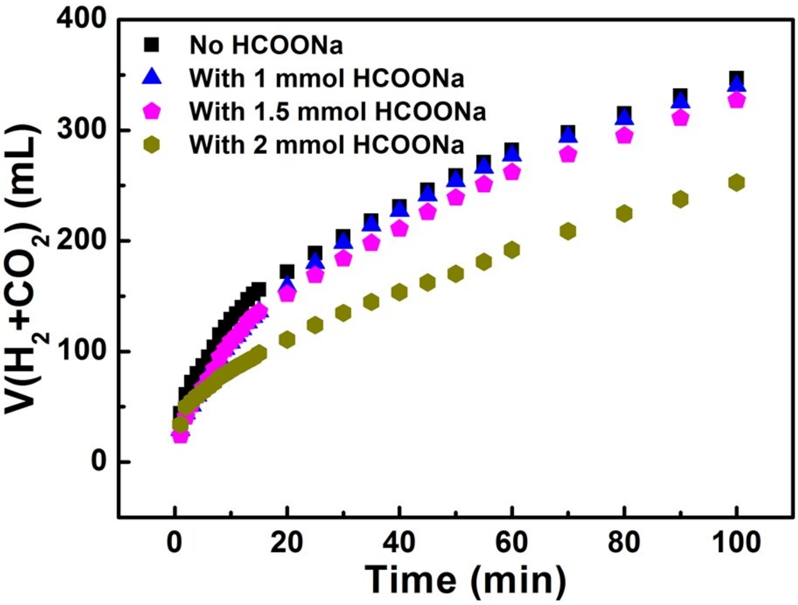

Figure S15. CO_2 + H_2 volume generated *vs.* time for the catalytic dehydrogenation of FA over PVPI-capped networked Pd_5Ag_5 NWs with or without sodium formate (SF) into catalytic system at 50 ^oC. Reaction conditions: 10 mmol FA (1 M), 50 ^oC and 20 mg catalyst.

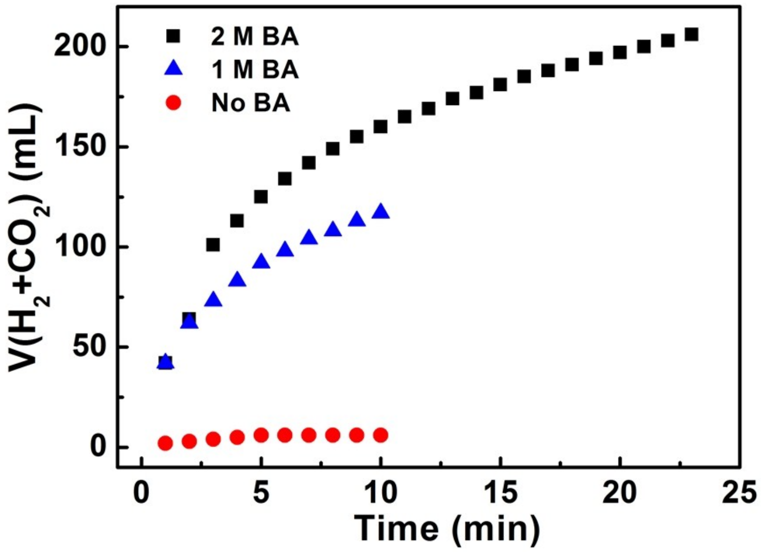

Figure S16. Decomposition of sodium formate catalyzed PVPI-capped networked Pd_5Ag_5 NWs with or without boric acid (BA) into catalytic system. Reaction conditions: 10 mmol SF (1 M), 80 ^oC and 20 mg catalyst.

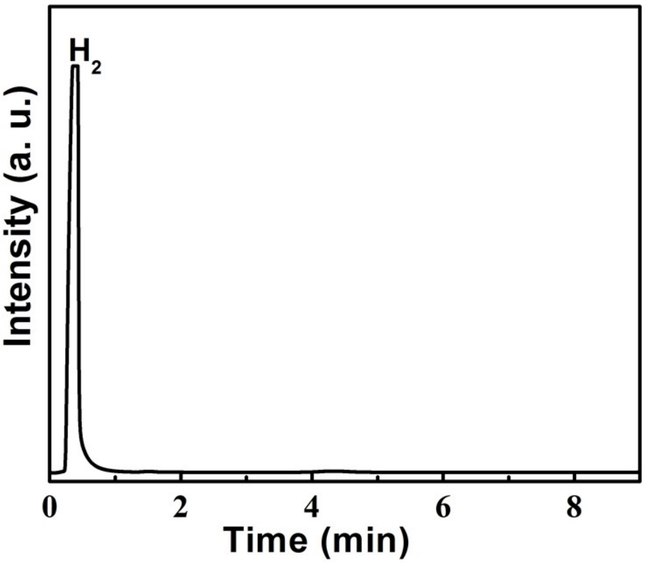

Figure S17. GC spectrum using TCD for the evolved gas from decomposition of sodium formate catalyzed PVPI-capped networked Pd_5Ag_5 NWs with boric acid (BA) into catalytic system. Reaction conditions: 10 mmol SF (1 M), 20 mmol BA (2 M), 80 °C, 20 mg catalyst.

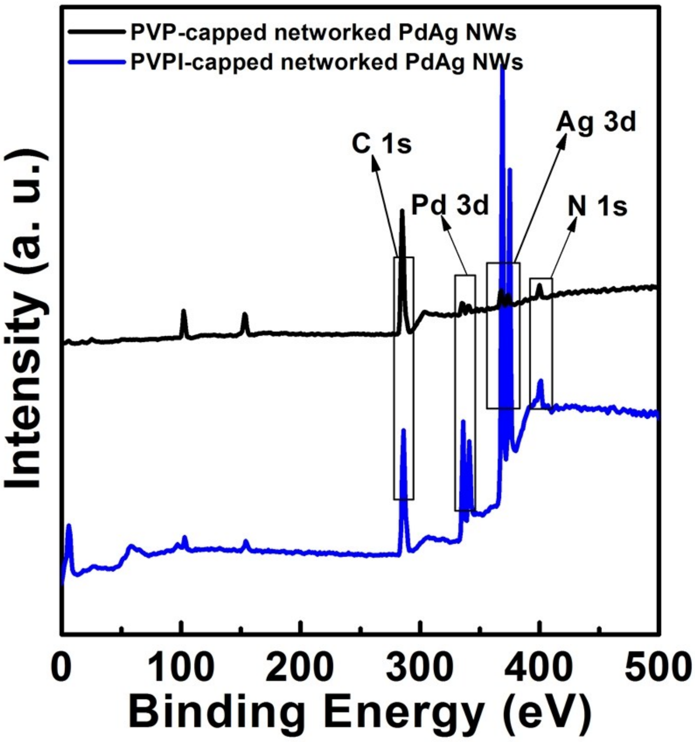

Figure S18. XPS spectra of PVPI-capped networked Pd_5Ag_5 NWs and PVP-capped networked Pd_5Ag_5 NWs.

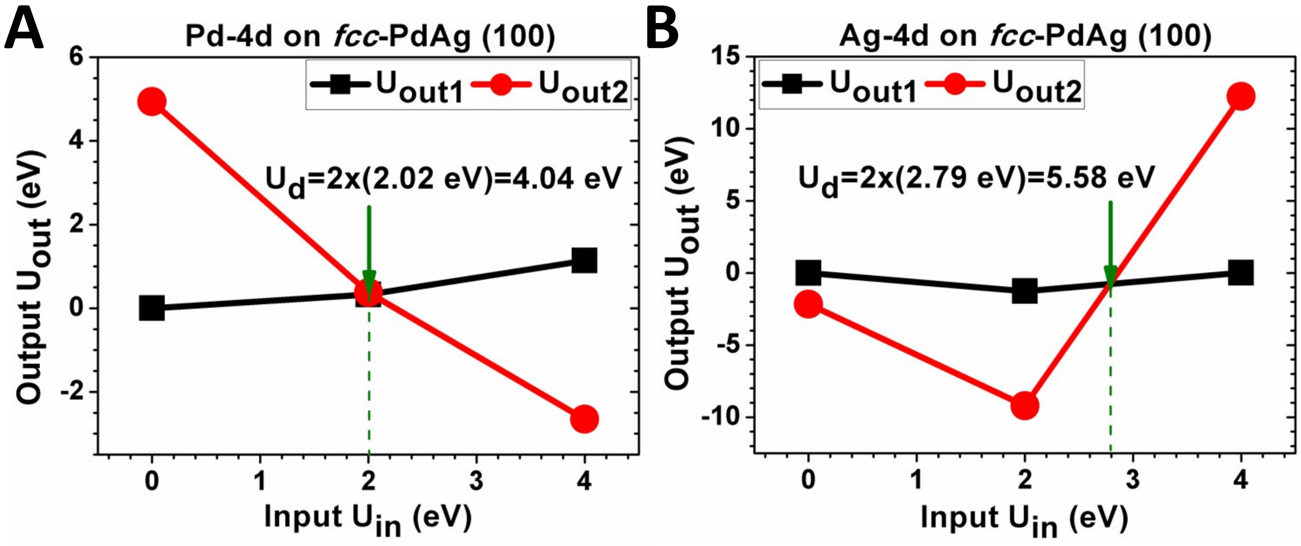

Figure S19. Obtained values of U_{out1} and U_{out2} for **(A)** 4*d* orbital of Pd on the (100) surface of PdAg within *fcc* lattice. **(B)** 4*d* orbital of Ag on the (100) of *fcc*-PdAg. The crossover feature indicates $|U_{\mathrm{out1}} - U_{\mathrm{out2}}| = 0$ denotes the fully occupied orbitals of 4*d* in both Pd and Ag sites on the (100) surface of fcc-PdAg.

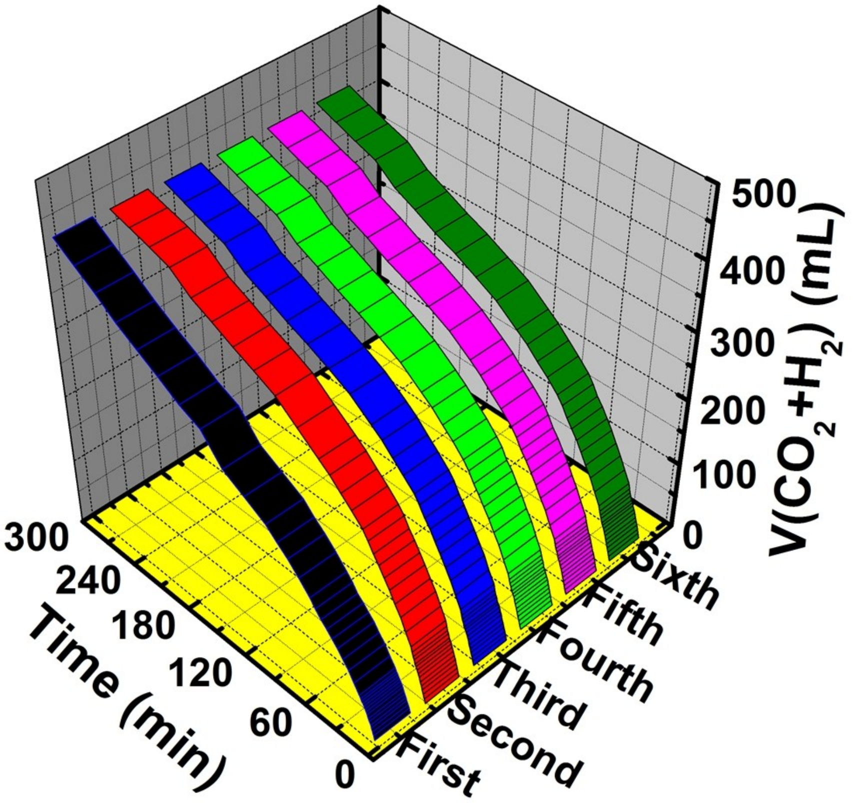

Figure S20. Reuse of the PVPI-capped networked Pd_5Ag_5 NWs catalyst for the catalytic FA dehydrogenation. Reaction conditions: aqueous FA solution (10 mL, 1 M), 25 °C and 20 mg catalyst.

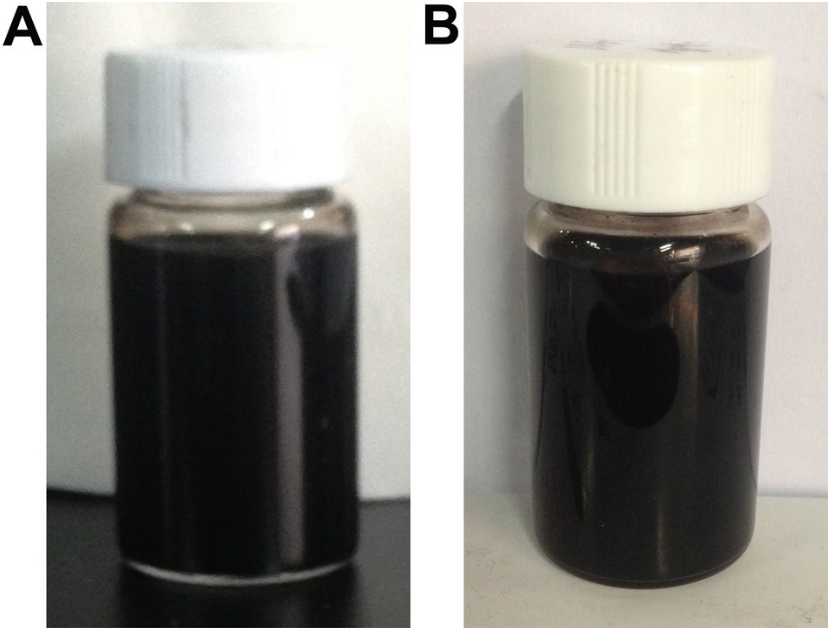

Figure S21. The photographs of PVPI-capped networked Pd_5Ag_5 NWs catalyst dispersed in aqueous solution **(A)** before and **(B)** after the sixth cycle. The catalytic stability of PVPI-capped networked Pd_5Ag_5 NWs was tested in aqueous FA solution (10.0 mL, 1.0 M) at 25 °C.

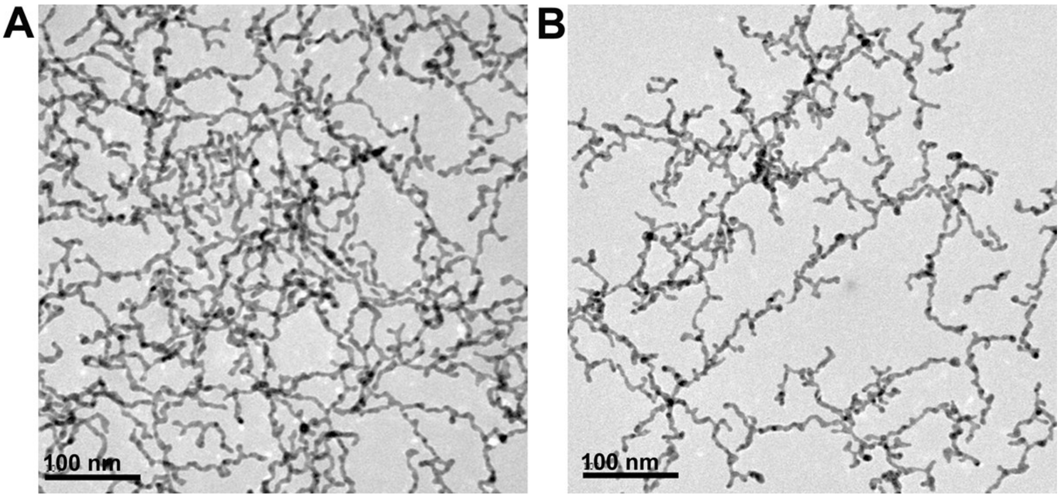

Figure S22. TEM image of the PVPI-capped networked Pd_5Ag_5 NWs catalyst (**A**) before and (**B**) after the sixth cycle.

Table S1 Elemental analysis results of PVPI-capped networked PdAg NWs catalyst characterized by inductively coupled plasma-atomic emission spectroscopy (ICP-OES).

Entry	$AgNO_3/Pd(NO_3)_2$ molar ratio	As-synthesized Networked NWs
1	7:3	Networked $Ag_{7.03}Pd_3$ NWs
2	5:5	Networked $Ag_{4.95}Pd_5$ NWs
3	3:7	Networked $Ag_{3.02}Pd_7$ NWs

Table S2 Initial TOF ($mol_{H2}\cdot mol\ catalyst^{-1}\ h^{-1}$) values for the decomposition of FA over various heterogeneous catalysts.

Catalyst	FA (mmol)	Additive (mmol)	Tem. (K)	$n_{Catalyst}$ (mmol)	$TOF_{initial}$	Recycle times	Ref.
Without support							
PVPI-capped Networked AgPd NWs	10.0	None	298	0.100	**242**	**6**	This work
PVPI-capped Networked AgPd NWs	10.0	None	323	0.100	**576**	**6**	This work
AgPd (1:1) NPs	10.0	None	323	0.200	**144.0**	—	22
Ag@Pd core-shell NPs	10.0	None	293	0.200	**15.5**	—	22
PdAg Nanosheets	10.0	HCOONa (5.0)	298	0.100	**156.0**	—	23
AgPd (41:59) NPs	10.0	None	298	0.100	**150.0**	—	24
With support							
$Ag_{42}Pd_{58}/C$	10.0	None	323	0.100	**382.0**	**4**	24
Ag@Pd/C	10.0	None	293	0.200	**192.0**	**2**	22
$Ag_{0.1}Pd_{0.9}/rGO$	5.0	HCOONa (3.35)	298	0.100	**105.2**	—	25
AgAuPd/rGO	5.0	None	298	0.100	**73.6**	—	26
AgPd-Hs/G	5.0	HCOONa (5.0)	298	0.100	**333.0**	**2**	27
CoAuPd/DNA-rGO	5.0	None	298	0.100	**85.0**	**3**	28

“**—,** —”For comparison, the cycle property of catalyst was not tested

Table S3 The PVPI-capped networked Pd_5Ag_5 NWs compositions before and after the sixth run characterized by inductively coupled plasma-atomic emission spectroscopy (ICP-OES).

Entry	Before the 6 catalytic run	After the 6 catalytic run
3	4.95:5	4.93:5

$TOF_{initial}$ calculation method:

$$x_a = \frac{\mathrm{Patm\ V'H2/\ RT}}{\mathrm{nFA}} \qquad \mathrm{S1^{f}}$$

Where x_a is conversion, P_{atm} is the atmospheric pressure, V'_{H2} is the final generated volume of H_2, R is the universal gas constant, T is room temperature (298 K), and n_{FA} is the mole number of FA.

$$TOF_{initial} = \frac{\mathrm{Patm\ V'H2/\ RT}}{\mathrm{nAg + Pd\ t}} \qquad \mathrm{S2}$$

Where $TOF_{initial}$ is initial turnover frequency, V'_{H2} is the generated volume of H_2 during the first 10 min of the reaction, n_{Ag+Pd} is the mole number of the Ag and Pd, and *t* is the reaction time of 10 min.

Supplementary References

1. Gu, X.; Lu, Z. H.; Jiang, H. L.; Akita, T.; Xu, Q., *J. Am. Chem. Soc.* **2011**, *133*, 11822.
2. Clark, S. J.; Segall, M. D.; Pickard, C. J.; Hasnip, P. J.; Probert, M. I. J.; Refson, K.; Payne, M. C., *Zeitschrift Fur Kristallographie* **2005**, *220*, 567.
3. Vladimir, I. A.; Aryasetiawan, F.; Lichtenstein, A. I., *J. Phys. Condens. Matter.* **1997,** *9*, 767.
4. Huang, B., *J. Comput. Chem.* **2016**, *37*, 825.
5. Huang, B.; Gillen, R.; Robertson, J., *J. Phys. Chem. C* **2014**, *118*, 24248.
6. Huang, B., *Philosophical Magazine* **2014**, *94*, 3052.
7. Huang, B., *Solid State Commun.* **2016**, *230*, 49.
8. Huang, B., *Solid State Commun.* **2016**, *237*, 34.
9. Huang, B., *Phys. Chem. Chem. Phys.* **2016**, *18*, 13564.
10. Marzari, N.; Vanderbilt, D.; Payne, M. C., *Phys. Rev. Lett.* **1997**, *79*, 1337.
11. Probert, M. I. J.; Payne, M. C., *Phys. Rev. B* **2003**, *67*, 075204.
12. Hasnip, P. J.; Pickard, C. J., *Comput. Phys. Commun.* **2006**, *174*, 24-29.
13. Laasonen, K.; Pasquarello, A.; Car, R.; Lee, C.; Vanderbilt, D., *Phys. Rev. B* **1993,** *47*, 10142.
14. Kleinman, L.; Bylander, D. M., *Phys. Rev. Lett.* **1982,** *48*, 1425.
15. Louie, S. G.; Froyen, S.; Cohen, M. L., *Phys. Rev. B* **1982**, *26*, 1738.
16. Grinberg, I.; Ramer, N. J.; Rappe, A. M., *Phys. Rev. B* **2000,** 62, 2311.
17. Rappe, A. M.; Rabe, K. M.; Kaxiras, E.; Joannopoulos, J. D., *Phys. Rev. B* **1990**, *41*, 1227.

18. Pickard, C. J.; Winkler, B.; Chen, R. K.; Payne, M. C.; Lee, M. H.; Lin, J. S.; White, J. A.; Milman, V.; Vanderbilt, D., *Phys. Rev. Lett.* **2000**, *85*, 5122.

19. Zacherle, T.; Schriever, A.; De Souza, R. A.; Martin, M., *Phys. Rev. B* **2013**, *87*, 134104.

20. Keating, P. R. L.; Scanlon, D. O.; Morgan, B. J.; Galea, N. M.; Watson, G. W., *J. Phys. Chem. C* **2011,** *116*, 2443.

21. Huang, B. *Phys. Chem. Chem. Phys.* **2017**, *19*, 8008.

22. Tedsree, K.; Li, T.; Jones, S.; Chan, C. W. A.; Yu, K. M. K.; Bagot, P. A. J.; Marquis, E. A.; Smith, G. D. W.; Tsang, S. C. E., *Nat. Nanotech.* **2011**, *6*, 302.

23. Hu, C. Y.; Mu, X. L.; Fan, J. M.; Ma, H. B.; Zhao, X. J.; Chen, G. X.; Zhou, Z. Y.; Zheng, N. F., *Chem. Nano. Mat.* **2016**, *2*, 28.

24. Zhang, S.; Metin, O.; Su, D.; Sun, S. H., *Angew. Chem. Int. Ed.* **2013**, *52*, 3681.

25. Ping, Y.; Yan, J. M.; Wang, Z. L.; Wang, H. L.; Jiang, Q., *J. Mater. Chem. A* **2013**, *1*, 12188.

26. Li, S. J.; Ping, Y.; Yan, J. M.; Wang, H. L.; Wu, M.; Jiang, Q., *J. Mater. Chem. A* 2015, **3**, 14535.

27. Jiang, Y. Q.; Fan, X. L.; Xiao, X. Z.; Qin, T.; Zhang, L. T.; Jiang, F. L.; Li, M.; Li, S. Q.; Ge, H. W.; Chen, L. X., *J. Mater. Chem. A* 2016, *4*, 657.

28. Wang, Z. L.; Wang, H. L.; Yan, J. M.; Ping, Y.; O, S. I.; Li, S. J.; Jiang, Q., *Chem. Commun.* 2014, *50*, 2732.